Graphene as transmissive electrodes and aligning layers for liquid-crystal-based electro-optic devices

Rajratan Basu* and Samuel A. Shalov
Department of Physics, Soft Matter and Nanomaterials Laboratory, The United States Naval Academy, Annapolis, Maryland 21402, USA
(Received 3 May 2017; published 10 July 2017)

In a conventional liquid crystal (LC) cell, polyimide layers are used to align the LC homogeneously in the cell, and transmissive indium tin oxide (ITO) electrodes are used to apply the electric field to reorient the LC along the field. It is experimentally presented here that monolayer graphene films on the two glass substrates can function concurrently as the LC aligning layers and the transparent electrodes to fabricate an LC cell, without using the conventional polyimide and ITO substrates. This replacement can effectively decrease the thickness of all the alignment layers and electrodes from about 100 nm to less than 1 nm. The interaction between LC and graphene through π-π electron stacking imposes a planar alignment on the LC in the graphene-based cell—which is verified using a crossed polarized microscope. The graphene-based LC cell exhibits an excellent nematic director reorientation process from planar to homeotropic configuration through the application of an electric field—which is probed by dielectric and electro-optic measurements. Finally, it is shown that the electro-optic switching is significantly faster in the graphene-based LC cell than in a conventional ITO-polyimide LC cell.

DOI: 10.1103/PhysRevE.96.012702

I. INTRODUCTION

Graphene (GP) [1] is a two-dimensional crystalline allotrope of carbon, where the carbon atoms are densely packed in a regular sp^2-bonded atomic-scale hexagonal pattern [2]. This two-dimensional material exhibits ballistic electron transport [3] and high optical transmittance [4], and therefore, it can be used as transparent electrodes in various electronic devices [5,6]. In another direction, liquid crystals (LCs) are widely used in electro-optical display technology due to their optical anisotropic properties. In liquid crystal displays (LCDs), the LC is contained inside capacitive semitransparent cells, where the two major components are the LC aligning layers and indium tin oxide (ITO) electrodes. The conventional LC aligning layer is a polyimide-coated surface where a unidirectional rubbing determines the nematic director ($\hat{n}$) profile of the LC in the cell. It has been shown before that graphene films can be used as the electrodes (instead of ITO) in an LC cell [5]. Here we report that a graphene-based LC cell can be fabricated without using any additional polyimide aligning layers or ITO electrodes. Graphene itself can be exploited simultaneously as the transparent electrodes and the LC aligning layers, obtaining excellent electro-optic effects of the LC, which is faster than that of the conventional ITO-polyimide LC cell.

II. PLANAR ALIGNMENT OF LC IN GRAPHENE-BASED CELL

It has been demonstrated that LC molecules can be stabilized on the *honeycomb* pattern of graphene [7,8] or carbon nanotubes [9–12], employing the π-π electron stacking with a binding energy of -2 eV. We first investigate the alignment mechanism of a nematic LC on a graphene film to understand the fundamental interaction between graphene and LC. Chemical vapor deposition (CVD) grown monolayer graphene film on a copper foil was obtained from Graphene Supermarket, Inc. The monolayer graphene from the copper foil was then transferred onto a $2.5 \times 2.5\,\text{cm}^2$ glass substrate using the polymethyl-methacrylate (PMMA) assisted transfer method [13,14]. A small droplet of E7 liquid crystal (obtained from EMD Millipore Corporation, $T_{\text{NI}} = 60.5\,^{\circ}\text{C}$) was placed on the graphene film and the droplet was then gently blown away by a dust blower to create a thin LC layer on the graphene surface situated on the glass substrate. The LC-coated graphene on the glass substrate was heated up in the isotropic phase to eliminate any residual order that resulted from the coating process and was then slowly cooled down to the nematic phase. The alignment of the LC on the graphene film was then studied by a crossed polarized microscope and the results are presented in Fig. 1.

Figures 1(a) and 1(b) illustrate the π-π stacking interaction that arises due to the overlap of the LC's benzene rings on the graphene-honeycomb structure. It is known that between two crossed polarizers, a *bright state* with the maximum transmitted intensity appears when the planar-aligned LC nematic director ($\hat{n}$) is at 45° with the polarizer (or with the crossed analyzer). A *dark state* is achieved if $\hat{n}$ is parallel to the polarizer (or to the crossed analyzer). Figure 1(a) schematically illustrates that the LC director ($\hat{n}$) on graphene is orientated at 45° with respect to the crossed polarizer and analyzer—which results in a bright state. When the system is rotated through 45°, the director ($\hat{n}$) orients parallel to the analyzer [see Fig. 1(b)]—which leads to a dark state. To observe these bright and dark states, the LC-coated graphene on the glass substrate was rotated over 180° under the crossed polarized microscope and the transmittance intensity was recorded. Figures 1(c)–1(e) show the micrographs ($0.35 \times 0.4\,\text{mm}^2$) of the LC-coated graphene on the glass substrate at three different relative angles, 55°, 78°, and 100°, respectively, of the substrate on the rotational microscope stage. These angles, however, are not the angles the nematic director ($\hat{n}$) makes with the crossed polarizers. Note that the difference in the angle between the bright state in Fig. 1(c) and dark state in Fig. 1(e) is 45°. Figure 1(f) shows the normalized

*basu@usna.edu

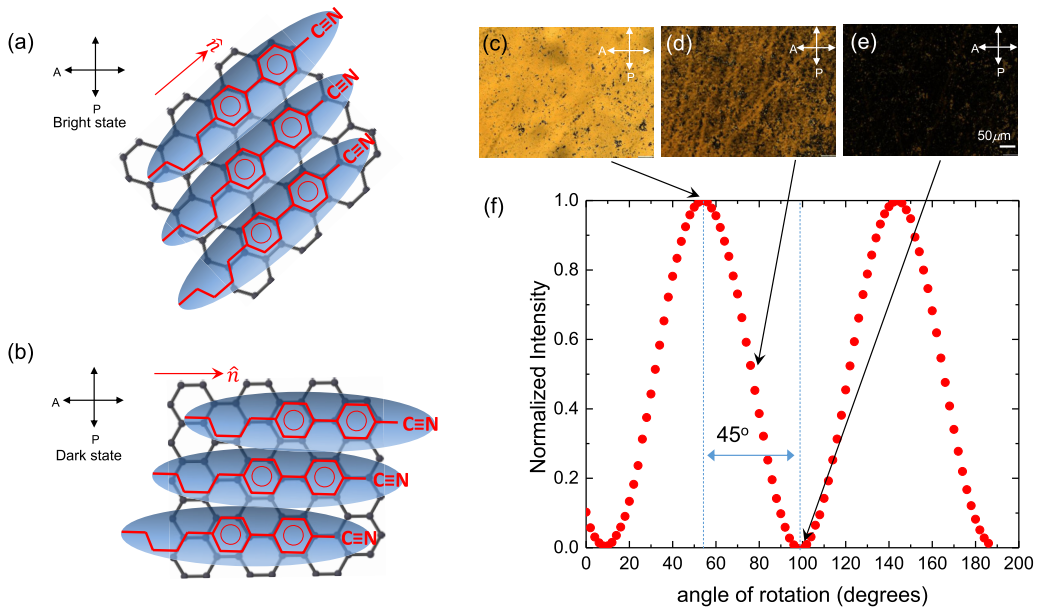

FIG. 1. (a) A schematic representation of the alignment of nematic LC molecules on graphene due to π-π electron stacking. The ellipsoids are LCs and the black honeycomb structure is the graphene surface. The LC molecular structure is shown in the ellipsoid on the graphene surface. The π-π electron stacking is illustrated by matching the LC's benzene rings on the graphene-honeycomb structure. The nematic director ($\hat{n}$) is orientated at 45° with respect to the crossed polarizer (P) and analyzer (A). This orientation, therefore, produces a bright state. (b) The system is rotated through 45° and the nematic director ($\hat{n}$) is parallel to A—which produces a dark state. (c–e) Microphotographs of a thin layer of nematic LC on a monolayer graphene film on a glass substrate under a crossed polarized microscope, showing a bright state, an intermediate state, and a dark state, respectively. (f) Normalized intensity as a function of the relative angle of rotation of the LC-coated graphene film on the glass substrate. The average director ($\hat{n}$) orientation for the microphotograph (c) is 45° with the crossed P and A—which produces a bright state. The average director ($\hat{n}$) orientation for the microphotograph (e) is 0° with P (or A)—which produces a dark state. The white bar in micrograph (e) presents 50 μm.

transmitted intensity as a function of the angle of rotation of the sample. The micrograph in Fig. 1(c) refers to the intensity at a 55° relative angle of rotation in Fig. 1(f), as shown by the arrow. Clearly, Fig. 1(c) exhibits a uniform *bright* texture of the LC—which suggests that the nematic director ($\hat{n}$) is at 45° with respect to the crossed polarizers. When the sample is rotated further through 45° [see Fig. 1(f) at 100° angle of rotation], the director ($\hat{n}$) becomes parallel to the polarizer or analyzer, clearly revealing a uniform *dark* texture in Fig. 1(e). Figure 1(d) shows an intermediate state ($45° < \theta < 90°$) of the director ($\hat{n}$). This transition of the transmitted intensity from bight to dark (or dark to bright) at every 45° rotation confirms that graphene imposes planar alignment on the nematic phase due to strong π-π electron stacking. In addition, these results suggest that the LC can achieve a uniform planar-aligned state over a large-scale dimension on graphene—which is essential for fabricating a graphene-based LC cell. However, note that even within a single graphene crystalline domain, the LC molecules can assume three different orientations separated by 60° disclination lines due to the hexagonal symmetry in the graphene crystal. There appears to be defectlike texture in graphene-aligned LC layers in Figs. 1(c)–1(e)—which, we believe, results from this alignment degeneracy of LC on graphene.

Two glass substrates with monolayer graphene film were used to prepare a cell. The two glass substrates were placed together (with the graphene sides facing each other) to make a cell with an average thickness of 13.5 μm. The graphene-based LC cell was then filled with E7 liquid crystal. To make a comparative study, a commercially available conventional 12-μm ITO-polyimide LC cell was also filled with E7 liquid crystal. Figure 2(a) schematically shows the ITO layers, polyimide alignment layers with rubbing direction, and the LC director ($\hat{n}$) orientation inside the conventional LC cell. Furthermore, Fig. 2(b) shows a picture of a conventional LC cell. The graphene-based LC cell is schematically presented in Fig. 2(c), and a picture of the cell is presented in Fig. 2(d). To achieve good electrical contact on the graphene surface, an electrically conductive epoxy was used as a solder replacement to prevent the graphene film from breaking away from the glass substrates. Figure 2(e) represents the Raman spectrum of graphene on the glass substrate—which confirms the presence of monolayer graphene film on the substrate.

The planar alignment of the LC in both cells was studied by rotating the cells over 180° under the crossed polarized microscope, and the results are presented in Fig. 3. The change in transmittance intensity of the conventional ITO-polyimide LC cell is depicted in Figs. 3(a)–3(c). The same change in the graphene-based LC cell is shown in Figs. 3(e)–3(h). Clearly, the transmittance intensity of the graphene-based cell in Fig. 3(h) and the conventional ITO-polyimide LC cell in Fig. 3(d) behave the same way, confirming a macroscopic planar alignment of the LC in the graphene-based cell. However, the LC texture in the graphene-based cell [Figs. 3(e)–3(g)] is remarkably different from that of the conventional

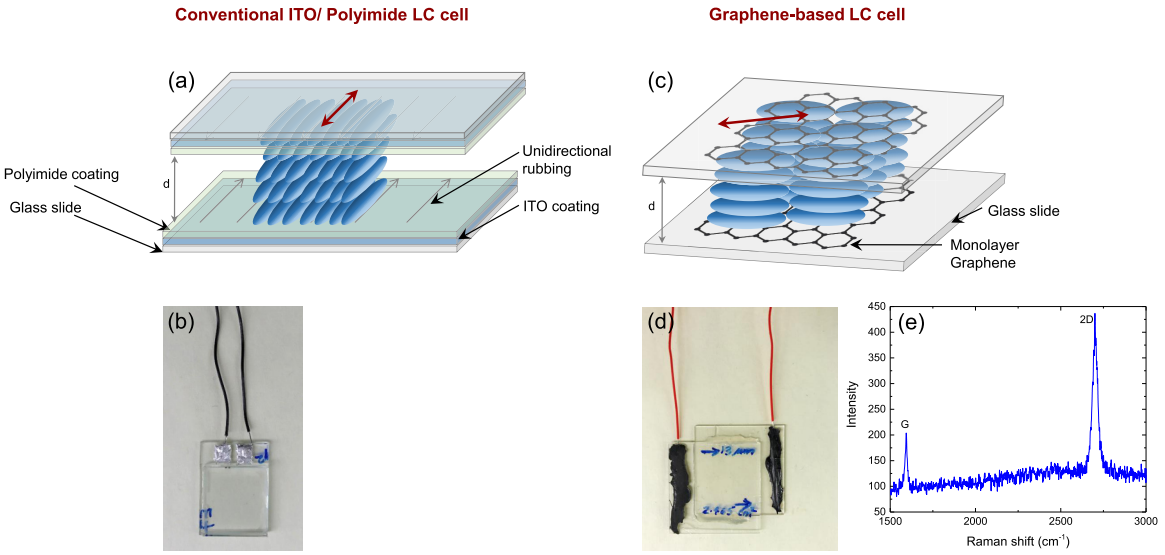

FIG. 2. (a) A schematic representation of a conventional LC cell containing a layer of ITO and a layer of polyimide coating with unidirectional rubbing on each glass slide, (b) the picture of a conventional LC cell, (c) a schematic representation of a graphene-based cell which contains a single layer of graphene on each glass slide, (d) the picture of a graphene-based LC cell, and (e) the Raman spectrum confirming the presence of the monolayer graphene on the glass substrate.

ITO-polyimide LC cell [Figs. 3(a)–3(c)]. This is because the graphene imposes planar alignment onto the LC molecules in a different mechanism than the polyimide alignment films. As discussed before, graphene imposes planar alignment on the nematic phase due to the strong π-π electron stacking. On the other hand, in conventional LC cells, the LC molecules align with alkyl side chains of the polyimide alignment film to generate planar alignment. The LC director ($\hat{n}$) orientation in the graphene-based cell in Fig. 3(e) is shown by the arrow at 45° with the crossed polarizers.

III. FIELD-INDUCED DIRECTOR REORIENTATION OF LC IN GRAPHENE-BASED CELL

The nematic phase shows dielectric anisotropy [15], $\Delta\varepsilon = \varepsilon_{\parallel} - \varepsilon_{\perp}$, where $\varepsilon_{\parallel}$ and $\varepsilon_{\perp}$ are the dielectric components parallel

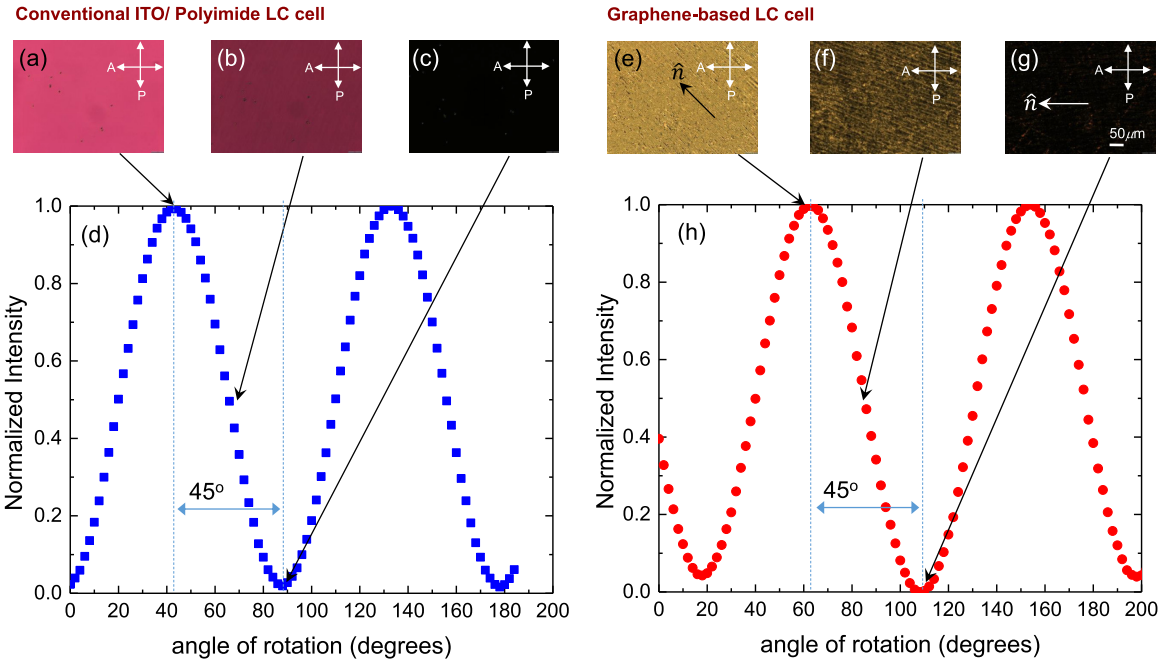

FIG. 3. (a–c) Micrographs of the bright, intermediate, and dark states, respectively, under the crossed polarized microscope of the conventional LC cell filled with E7 liquid crystal; (d) normalized transmitted intensity as a function of the relative angle of rotation for the conventional LC cell; (e–g) micrographs of the bright, intermediate, and dark states, respectively, under the crossed polarized microscope of the graphene-based LC cell filled with E7 liquid crystal; (h) normalized transmitted intensity as a function of the relative angle of rotation for the graphene-based LC. The white bar in micrograph (g) presents 50 μm.

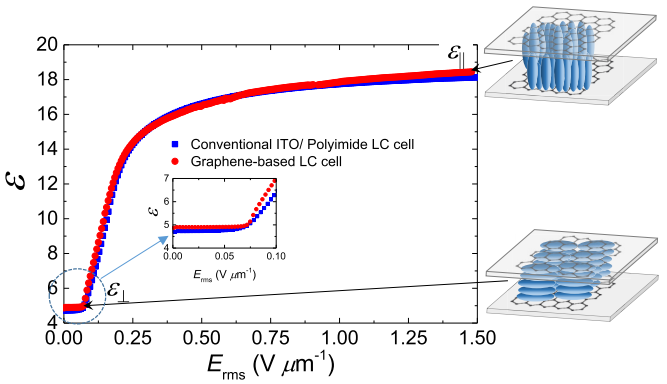

FIG. 4. Dielectric constant ε as a function of applied rms field $\vec{E}$ ($f = 1000$ Hz) in the nematic phase ($T = 22\,^{\circ}$C) of E7 liquid crystal in two different LC cells listed in the legend. This shows that the LC can exhibit a typical Fréedericksz transition in the graphene-based LC cell. The inset shows that the threshold field in the graphene-based cell is more than that of the conventional cell.

and perpendicular to the nematic director ($\hat{n}$), respectively. In a uniform planar-aligned parallel-plate cell configuration, the nematic director ($\hat{n}$) of a positive anisotropic ($+\Delta\varepsilon$) LC is initially aligned perpendicular to the applied electric field $\vec{E}$, but the director can reorient parallel to $\vec{E}$ if the field magnitude is above some critical threshold. The reorientation process of the nematic director ($\hat{n}$) occurs because the director experiences a torque $\propto\Delta\varepsilon E^2$ in the presence of $\vec{E}$. This is the essence of the Fréedericksz transition, and the dielectric measurement as a function of the applied field across the cell can reveal this LC reorientation process.

E7 liquid crystal is a positive anisotropic LC with $\Delta\varepsilon = +13.8$ [16]. An automatic liquid crystal tester (Instec, Inc.) was employed to measure the dielectric constant of E7 liquid crystal as a function of the applied ac electric field at 1000 Hz in the nematic phase ($T = 22\,^{\circ}$C), in both the conventional ITO-polyimide cell and graphene-based cell. The ac field (and not dc) was applied to prevent the effect of ion migration from influencing the dielectric measurements. The dielectric constant as a function of the applied field for both cells is presented in Fig. 4. The purpose of this experiment is to demonstrate that graphene can be utilized as conducting electrodes. The dielectric constant of E7 as a function of the applied field in the graphene-based cell clearly exhibits the Fréedericksz transition similar to that of the conventional ITO-polyimide cell, confirming graphene's capability of being used as electrodes. In the graphene-based cell, $\Delta\varepsilon = +13.57$, while in the conventional ITO-polyimide cell, $\Delta\varepsilon = +13.49$. These values are within 2% of the reported value of $\Delta\varepsilon$ for E7 liquid crystal [16]. Thus, this experiment confirms that the LC director ($\hat{n}$) can reorient from planar to homeotropic configuration in the graphene-based cell in the presence of $\vec{E}$. These results also demonstrate that graphene itself can be exploited as the electrodes as well as the aligning layers in a cell without having any ITO and polyimide layers.

A careful observation also reveals that the *threshold electric field* to start the reorientation process is higher in the graphene-based cell. See the inset in Fig. 4. The capacitance measurement shows that $V_{\rm th}^{\rm graphene\ cell} = 0.971$ V and $V_{\rm th}^{\rm ITO-polyimide\ cell} = 0.841$ V. The polar anchoring strength coefficient, $W_\theta \propto V_{\rm th}^2$ [17]. This suggests that W_θ is higher in the graphene-based cell. This is because the LC-graphene interaction is stronger than the LC-polyimide interaction, and therefore, a higher field is required to overcome the anchoring energy of the LC at the graphene surface.

The dielectric (capacitive) data for the graphene-based cell have been used to extract the bend (K_{33}) and splay (K_{11}) elastic constants using the Fréedericksz transition method [18] by fitting the capacitance (C) vs voltage (V) graphs according to the equation $\frac{C}{C_o} = \frac{2}{\pi}\sqrt{1+\gamma\sin^2\varphi_m}\frac{V_{th}}{V}\int_{\varphi_0}^{\varphi_m}\sqrt{\frac{(1+\gamma\sin^2\varphi)(1+\kappa\sin^2\varphi)}{\sin^2\varphi_m-\sin^2\varphi}}d\varphi$, where $C_{\rm o}$ is the zero-field capacitance, φ is the angle between the director and the substrate at V, $\varphi_{\rm m}$ is the maximum angle in the middle of the cell, $\varphi_{\rm o}$ is the pretilt angle, $\gamma = \Delta\varepsilon/\varepsilon_\perp$, $\kappa = (K_{33}/K_{11})$–1, and $V_{\rm th}$ is the threshold voltage. From this fitting, $K_{33} = 20.1$ pN and $K_{11} = 11.4$ pN—these values are within 4% of the reported values of K_{33} and K_{11} for E7 liquid crystal [16]. The extracted values of K_{33} and K_{11} suggest that the graphene-based cell can be used reliably to characterize a nematic LC.

IV. ELECTRO-OPTIC EFFECT OF LC IN GRAPHENE-BASED CELL

The electrically controlled birefringence effect in an LC [19] is observed when the applied field exceeds its threshold value and the nematic director deviates from the initial planar orientation to homeotropic orientation in the cell, changing its effective birefringence $\langle\Delta n\rangle$ as a function of applied voltage. If the nematic director is initially oriented at 45° with the crossed polarizers, then the transmitted intensity at the exit of the analyzer can be written as [19]

$$I = I_o\sin^2\left(\frac{\pi d\langle\Delta n\rangle}{\lambda}\right), \tag{1}$$

where $I_{\rm o}$ is the intensity of the plane polarized light incident on the LC cell, d is the cell thickness, and λ is the wavelength of the monochromatic light. As the director rotates in the presence of the applied field, a change in the phase difference, $\Delta\phi = \frac{2\pi d\langle\Delta n\rangle}{\lambda}$, results in an oscillatory dependence of the optical signal at the exit of the analyzer.

The electrically controlled birefringence effect of the LC in the graphene-based cell was studied from the electro-optic response of the cell. The optical setup consisted of a beam from a 5-mW He-Ne laser at wavelength 633 nm that passed through a polarizer, the graphene-based LC cell, a crossed analyzer, and into a nanosecond Newport photodetector. The incident beam was polarized at an angle of 45° with respect to the nematic director of the LC in the graphene-based cell. The output of the detector was fed into a dc voltmeter, allowing us to measure the transmitted intensity I. The applied ac voltage at 1000 Hz was ramped up across the cell and the change in the transmitted intensity was detected by the dc voltmeter. The setup was computer controlled and data acquisition was performed using LABVIEW® software. This experiment was also repeated under the crossed polarized microscope, and several micrographs of the graphene-based cell were taken at different applied voltages.

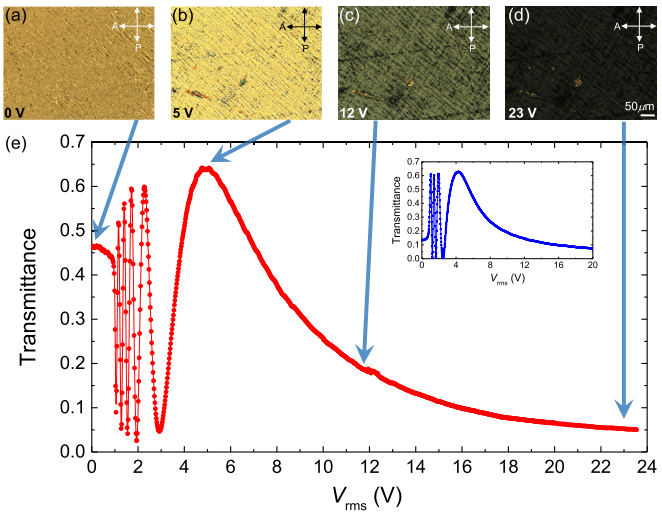

FIG. 5. Electrically controlled birefringence effect of E7 liquid crystal in the graphene-based cell. (a–d) Micrographs of the graphene-based LC cell filled with E7 liquid crystal under the crossed polarized microscope at 0, 5, 12, and 23 V, respectively. (e) The transmittance $\frac{I}{I_o}$ of E7 liquid crystal ($T = 22\,^{\circ}$C) in the graphene-based cell as a function of applied ac voltage ($f = 1000$ Hz). The inset shows the transmittance of E7 liquid crystal in the conventional ITO-polyimide cell as a function of applied ac voltage ($f = 1000$ Hz). The white bar in micrograph (d) presents 50 μm.

Figure 5 represents the electrically controlled birefringence effect of E7 liquid crystal in the graphene-based cell. Figures 5(a)–5(d) show the micrographs of the LC texture in the graphene-based cell at 0, 5, 12, and 23 V, respectively. Figure 5(e) exhibits the transmittance $\frac{I}{I_o}$ of E7 liquid crystal in the graphene-based cell as a function of the applied ac voltage. This transmittance clearly follows the oscillatory behavior according to Eq. (1). The number of oscillations (i.e., the number of maxima during a complete reorientation of the director) in the transmittance vs voltage curve of Fig. 5(e) is approximately $\frac{d}{\lambda}\frac{\Delta n}{}$ [19]. Now, using $d = 13.5\,\mu$m for the graphene-based cell, $\lambda = 633$ nm for the He-Ne laser, and $\Delta n = 0.225$ for E7 liquid crystal, $\frac{d\Delta n}{\lambda} \approx 5$. The transmittance vs voltage curve for the graphene-based cell clearly shows *five* maxima in Fig. 5(e). The inset in Fig. 5(e) presents the transmittance of E7 liquid crystal in the conventional ITO-polyimide cell for reference. The results indicate that the graphene-based cell exhibits an excellent electrically controlled birefringence effect—where graphene itself concurrently acts as the alignment layers and the transparent electrodes at the two glass substrates. The contrast ratio $\frac{I_{max}}{I_{min}}$, however, shows a 15% drop in the graphene-based cell.

V. ELECTRO-OPTIC SWITCHING TIMES OF NEMATIC LC IN GRAPHENE-BASED CELL

In this section, the electro-optic time responses of the nematic LC in the graphene-based cell are investigated. The two characteristic times [20], rise (voltage on) and decay (voltage off), of the nematic director, can be described as

$$\tau_{\text{rise}} = \frac{\gamma_1 d^2}{\Delta\varepsilon\varepsilon_o V^2 - K_{11}\pi^2}, \quad \tau_{\text{decay}} = \frac{\gamma_1 d^2}{K_{11}\pi^2}, \qquad (2)$$

where γ_1 is the rotational viscosity, d is the cell thickness, ε_0 the is free space permittivity, K_{11} is the splay elastic constant, and V is the applied voltage. τ_{rise} is the time the nematic director ($\hat{n}$) takes to rotate from planar to homeotropic configuration, when the voltage is turned on across a planar-aligned cell. Similarly, τ_{decay} is the time the director takes to rotate back from homeotropic to planar configuration after the voltage is turned off.

The field-induced nematic switching times were studied from the electro-optic responses of the LC cells. The optical setup consisted of a beam from a 5-mW He-Ne laser at a wavelength of 633 nm that passed through a polarizer, the graphene-based cell, a crossed analyzer, and into a nanosecond Newport photodetector. See Fig. 6(a). The beam was polarized at an angle of 45° with respect to the nematic director ($\hat{n}$). The output of the detector was fed into a digital storage oscilloscope. A dc voltage pulse at a pulse interval of 20 Hz was applied across the cell and the change in transmitted intensity as a function of time (both when the voltage was turned on and off) was detected by the oscilloscope. Transmittance responses for the field when turned on and off were studied for several applied voltages much higher than the threshold switching voltage. The setup was computer controlled and data acquisition was performed using LABVIEW® software.

Figure 6(b) represents the normalized transmitted intensity responses of E7 liquid crystal in both the graphene-based cell and the conventional ITO-polyimide cell as a function of time for a voltage (27 V) that was turned on and off. The black dashed line at the top of the graph shows the applied voltage profile. At $t = 0$, the applied voltage is turned off, and the transmitted intensity increases as a function of time. The time the transmitted intensity takes to rise from 10% to 90% of the maximum intensity after the voltage is turned off is defined as the optical switching off, τ_{off}. At $t = 25$ ms, the applied voltage is turned on, and the transmitted intensity drops as a function of time. The time the transmitted intensity takes to drop from 90% to 10% of the maximum intensity after the voltage is turned on is defined as the optical switching on, τ_{on}. Note that τ_{rise} and τ_{decay} [Eq. (2)] are not equal to the electro-optical responses—τ_{on} and τ_{off}, respectively. The optical response is mainly due to the director's rotation after the field is turned on or off. Therefore, one can write $\tau_{\text{rise}} \propto \tau_{\text{on}}$ and $\tau_{\text{decay}} \propto \tau_{\text{off}}$, neglecting the backflow in the cell.

The top panel in Fig. 6(c) shows τ_{on} as a function of applied peak-to-peak voltage, V_{pp}, for E7 liquid crystal in both the cells. Similarly, the bottom panel in Fig. 6(c) shows τ_{off} as a function of V_{pp} for E7 liquid crystal in both the cells. Note that τ_{on}, $\tau_{\text{off}} \propto d^2$ [Eq. (2)]; i.e., a thicker cell exhibits a slower response for the same LC. In this experiment, the graphene-based cell ($d_{\text{graphene-cell}} = 13.5\,\mu$m) is thicker than the conventional ITO-polyimide cell ($d_{\text{ITO-cell}} = 12\,\mu$m). It is apparent that τ_{on} for the graphene-based cell is faster despite the cell being thicker than the ITO-polyimide cell. Now, if τ_{off} for the ITO-polyimide cell is scaled to that of a cell with a thickness of 13.5 μm(=$d_{\text{graphene-cell}}$), i.e., $\tau_{\text{off\_scaled}} = \tau_{\text{off}}$ (for ITO-polyimide cell)$\times \frac{d^2_{\text{graphene-cell}}}{d^2_{\text{ITO-cell}}}$, then $\tau_{\text{off\_scaled}} > \tau_{\text{off\_graphene-cell}}$ from the data shown in the bottom panel of Fig. 6(c). This indicates that for the same cell

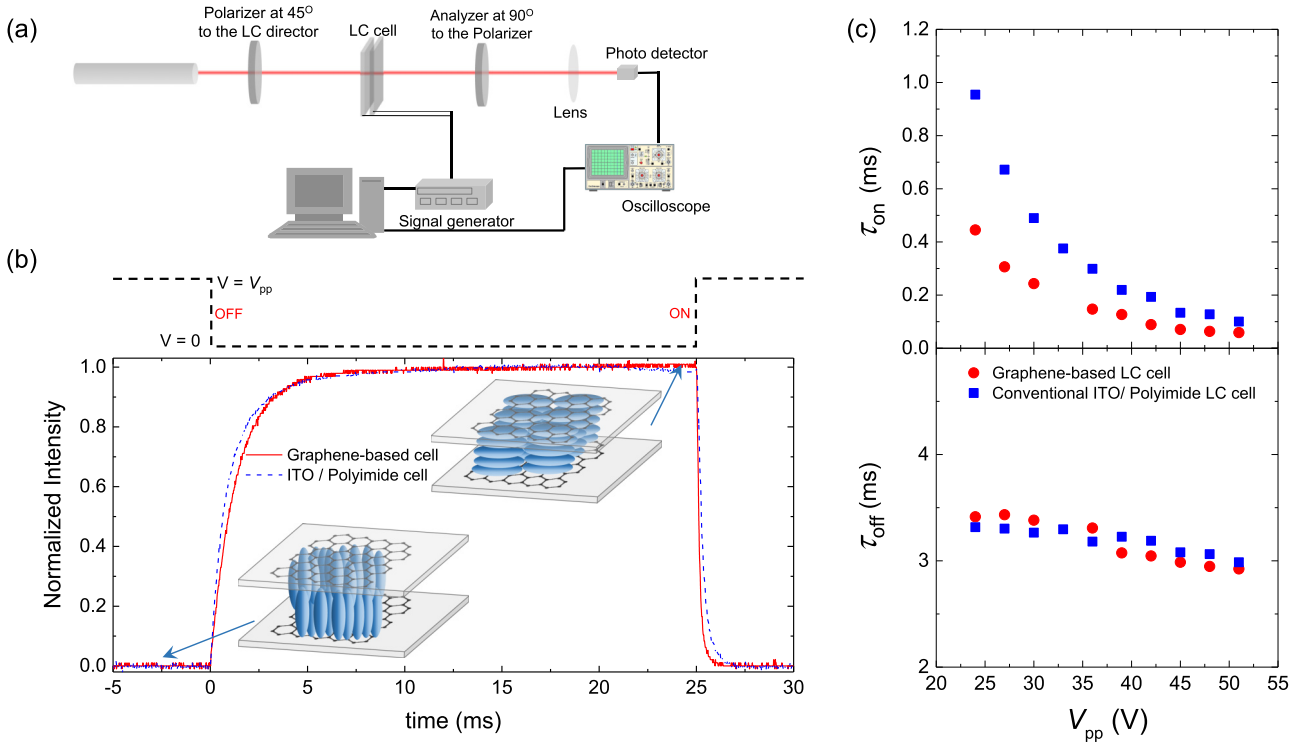

FIG. 6. Electro-optical switching of E7 liquid crystal in the graphene-based cell. (a) A schematic presentation of the experimental setup. (b) Normalized transmitted intensity as a function of time when a peak-to-peak voltage ($V_{pp} = 27$ V) is turned off at $t = 0$, and then turned on at $t = 25$ ms, for the two cells listed in the legend ($T = 22\,^{\circ}$C). The dashed line represents the applied voltage profile. (c) Top panel: τ_{on} as a function of V_{pp} for E7 liquid crystal for the two cells listed in the legend. Bottom panel: τ_{off} as a function of V_{pp} for E7 liquid crystal for the two cells listed in the legend.

thickness, τ_{off} for the graphene-based cell is faster than that of the ITO-polyimide cell. Thus, not only does the graphene-based cell exhibit excellent nematic switching, the switching responses, τ_{on} and τ_{off}, are also significantly accelerated in this cell.

Several reports in the literature show that that the presence of carbon nanomaterials (such as carbon nanotubes, graphene flakes, fullerenes) in liquid crystals can significantly reduce the free-ion concentration in the LC media [21–23] by the ion-trapping process. The diminished presence of free ions can reduce the internal friction, resulting in a decrease in the rotational viscosity γ_1 of the LC media [24–27]. The response times, τ_{rise} and τ_{decay}, linearly depend on γ_1 [Eq. (2]. A reduction in γ_1, therefore, causes a faster rotation of the LC molecules [21,23,26]. In particular, the presence of graphene flakes in colloidal form in an LC allows the LC to respond quicker upon application of an external field [23–26]. In the graphene-based cell, the LC is exposed to a $2 \times 2.5\,\text{cm}^2$ graphene-coated surface area. It is possible that during the filling process of the cell, the graphene films at the two surfaces trap some ions from the LC and reduce the free-ion concentration in LC, decreasing γ_1—hence the observed accelerated responses for τ_{on} and τ_{off} in the graphene-based cell.

VI. CONCLUSION

It is demonstrated that monolayer graphene can function as the alignment layers and the electrodes simultaneously, showing a typical Fréedericksz transition upon the application of an electric field across the LC cell. The measured LC parameters, such as $\Delta\varepsilon$, K_{33}, K_{11}, using the graphene-based cell are found to be within the acceptable range of the reported values of the LC. The graphene-based LC cell exhibits excellent electro-optic effects with accelerated response times. Additionally, the total thickness of all the alignment layers and electrodes in a conventional ITO-polyimide cell is about 100 nm or more [28]. The thickness of a monolayer graphene film is around 0.37 nn [26]. Replacing both the layers with monolayer graphene reduces this effective thickness to less than 1 nm. Reducing this effective thickness could offer the potential to minimize the transmissive losses and optimize throughput of light over a wide range of spectral bands for modern LC devices. Presented results are expected to advance the conceptions about, and methodology toward, nanoscale manipulation LCs and LC orientation control using their interactions with graphene. These studies will not only make liquid crystal technologically useful (i.e., faster switching), but will also directly lead to the central role played by the LC-graphene interaction at the nanoscale interface and its effect at the macroscopic level.

ACKNOWLEDGMENTS

This work was supported by the Office of Naval Research (Award No. N0001417WX01519) and the investment grant at the U.S. Naval Academy.

[1] K. S. Novoselov, A. K. Geim, S. V. Morozov, D. Jiang, Y. Zhang, S. V. Dubonos, I. V. Grigorieva, and A. A. Firsov, Electric field effect in atomically thin carbon films, Science **306**, 666 (2004).

[2] J. C. Meyer, A. K. Geim, M. I. Katsnelson, K. S. Novoselov, T. J. Booth, and S. Roth, The structure of suspended graphene sheets, Nature **446**, 60 (2007).

[3] A. K. Geim and K. S. Novoselov, The rise of graphene, Nat. Mater. **6**, 183 (2007).

[4] R. R. Nair, P. Blake, A. N. Grigorenko, K. S. Novoselov, T. J. Booth, T. Stauber, N. M. R. Peres, and A. K. Geim, Fine structure constant defines visual transparency of graphene, Science **320**, 1308 (2008).

[5] P. Blake, P. D. Brimicombe, R. R. Nair, T. J. Booth, D. Jiang, F. Schedin, L. A. Ponomarenko, S. V. Morozov, H. F. Gleeson, E. W. Hill, A. K. Geim, and K. S. Novoselov, Graphene-based liquid crystal device, Nano Lett. **8**, 1704 (2008).

[6] X. Wang, L. Zhi, and K. Mullen, Transparent, conductive graphene electrodes for dye-sensitized solar cells, Nano Lett. **8**, 323 (2008).

[7] D. W. Kim, Y. H. Kim, H. S. Jeong, and H. T. Jung, Direct visualization of large-area graphene domains and boundaries by optical birefringency, Nat. Nanotechnol. **7**, 29 (2012).

[8] M. A. Shehzad, D. H. Tien, M. W. Iqbal, J. Eom, J. H. Park, C. Hwang, and Y. Seo, Nematic liquid crystal on a two dimensional hexagonal lattice and its application, Sci. Rep. **5**, 13331 (2015).

[9] K. A. Park, S. M. Lee, S. H. Lee, and Y. H. Lee, Anchoring a liquid crystal molecule on a single-walled carbon nanotube, J. Phys. Chem. C **111**, 1620 (2007).

[10] R. Basu and A. Garvey, Insulator-to-conductor transition in liquid crystal-carbon nanotube nanocomposites, J. Appl. Phys. **120**, 164309 (2016).

[11] R. Basu and G. S. Iannacchione, Orientational coupling enhancement in a carbon nanotube dispersed liquid crystal, Phys. Rev. E **81**, 051705 (2010).

[12] R. Basu, K. Boccuzzi, S. Ferjani, and C. Rosenblatt, Carbon nanotube induced chirality in an achiral liquid crystal, Appl. Phys. Lett. **97**, 121908 (2010).

[13] X. Li, Y. Zhu, W. Cai, M. Borysiak, B. Han, D. Chen, R. D. Piner, L. Colombo, and R. S. Ruoff, Transfer of large-area graphene films for high-performance transparent conductive electrodes, Nano Lett. **9**, 4359 (2009).

[14] X. Liang, B. A. Sperling, I. Calizo, G. Cheng, C. A. Hacker, Q. Zhang, Y. Obeng, K. Yan, H. Peng, Q. Li, X. Zhu, H. Yuan, A. R. H. Walker, Z. Liu, L.-M. Peng, and C. A. Richter, Toward clean and crackless transfer of graphene, ACS Nano **5**, 9144 (2011).

[15] P. G. De Gennes and J. Prost, *The Physics of Liquid Crystals* (Oxford University Press, New York, 1995).

[16] licristal® E7 Data Sheet, Merck KGaA, Germany, 2001.

[17] A. Murauski, V. Chigrinov, A. Muravsky, F. S.-Y. Yeung, J. Ho, and H.-S. Kwok, Determination of liquid-crystal polar anchoring energy by electrical measurements, Phys. Rev. E **71**, 061707 (2005).

[18] D. Demus, J. Goodby, G. W. Gary, H.-W. Spiess, and V. Vill, *Physical Properties of Liquid Crystals* (Wiley-VCH, Weinheim, Germany, 1999).

[19] L. M. Blinov and V. G. Chigrinov, *Electro-optic Effects in Liquid Crystal Materials* (Springer-Verlag, New York, 1996).

[20] E. Jakeman and E. P. Raynes, Electro-optic response times in liquid crystals, Phys. Lett. A **39**, 69 (1972).

[21] H. Y. Chen, W. Lee, and N. A. Clark, Faster electro-optical response characteristics of a carbon-nanotube-nematic suspension, Appl. Phys. Lett. **90**, 033510 (2007).

[22] C. -W. Lee and W. -P. Shih, Quantification of ion trapping effect of carbon nanomaterials in liquid crystals, Mater. Lett. **64**, 466 (2010).

[23] R. Basu, A. Garvey, and D. Kinnamon, Effects of graphene on electro-optic response and ion-transport in a nematic liquid crystal, J. Appl. Phys. **117**, 074301 (2015).

[24] R. Basu, D. Kinnamon, and A. Garvey, Nano-electromechanical rotation of graphene and giant enhancement in dielectric anisotropy in a liquid crystal, Appl. Phys. Lett. **106**, 201909 (2015).

[25] R. Basu, Effects of graphene on electro-optic switching and spontaneous polarization of a ferroelectric liquid crystal, Appl. Phys. Lett. **105**, 112905 (2014).

[26] R. Basu, D. Kinnamon, N. Skaggs, and J. Womak, Faster in-plane switching and reduced rotational viscosity characteristics in a graphene-nematic suspension, J. Appl. Phys. **119**, 185107 (2016).

[27] R. Basu, D. Kinnamon, and A. Garvey, Graphene and liquid crystal mediated interactions, Liq. Cryst. **43**, 2375 (2016).

[28] M. Jiao, Z. Ge, Q. Song, and S.-T. Wu, Alignment layer effects on thin liquid crystal cells, Appl. Phys. Lett. **92**, 061102 (2008).